Supporting Information: A Route to High Performance Micro-Solid Oxide Fuel Cells on Metallic Substrates

Matthew P. Wells[*1], Adam J. Lovett[1], Thomas Chalklen[1], Federico Baiutti[2], Albert Tarancón,[2,3] Xuejing Wang[4], Jie Ding[4], Haiyan Wang[4], Sohini Kar-Narayan[1], Matias Acosta[1], Judith L. MacManus-Driscoll[1]*

[1]Department of Materials Science and Metallurgy, University of Cambridge, 27 Charles Babbage Road, Cambridge CB3 0FS, United Kingdom.

[2]Catalonia Institute for Energy Research (IREC), Department of Advanced Materials for Energy, 1 Jardins de les Dones de Negre, Barcelona 08930, Spain.

[3]ICREA, 23 Passeig Lluís Companys, Barcelona 08010, Spain

[4]School of Materials Engineering, Purdue University, 701 West Stadium Avenue, West Lafayette, Indiana, 47907-2045, United States.

*** Corresponding Author: mpw52@cam.ac.uk**

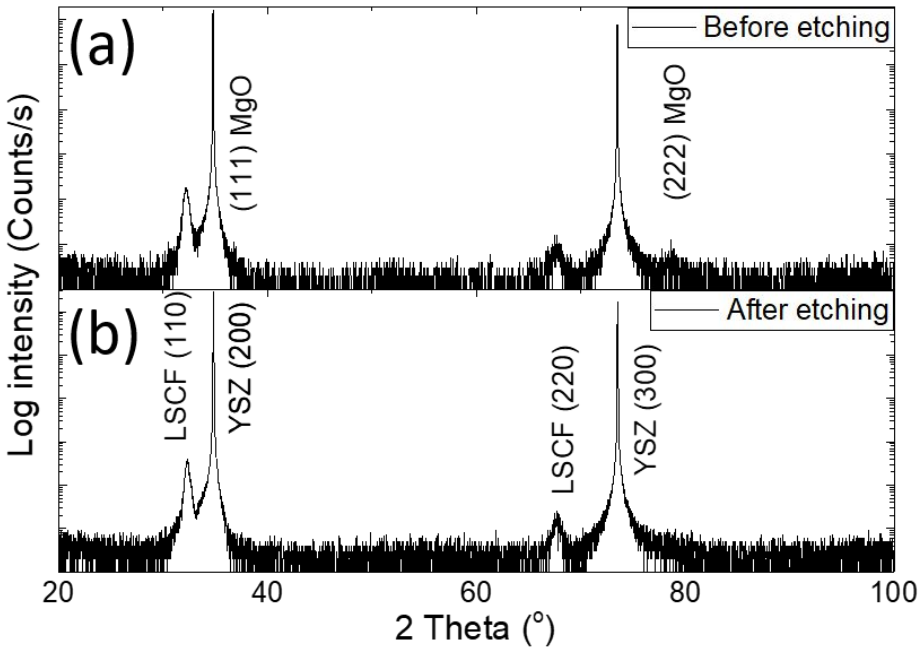

Figure S1: XRD measurements of LSCF/MgO cathode on single-crystal YSZ a) before and b) after etching

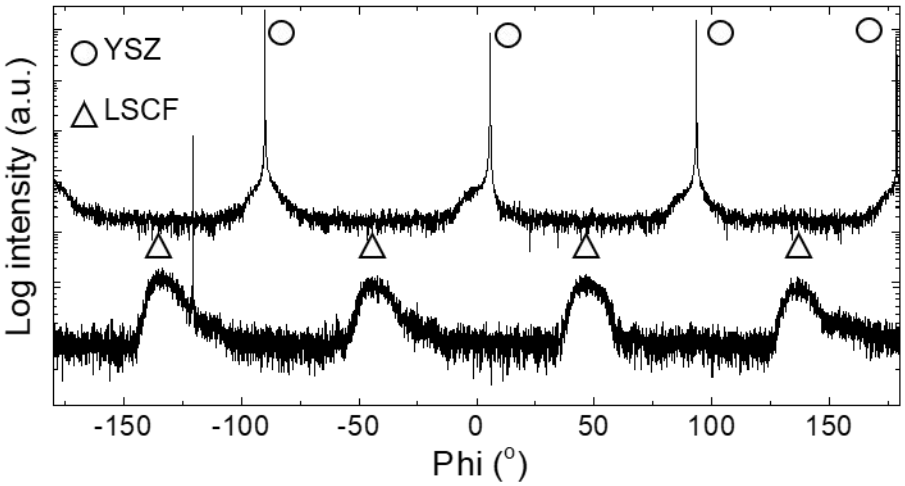

Figure S2: In-plane (Phi) scans for 70 nm unetched VAN LSCF film on single crystal YSZ about the LSCF 12-1 and YSZ 31-1 peaks

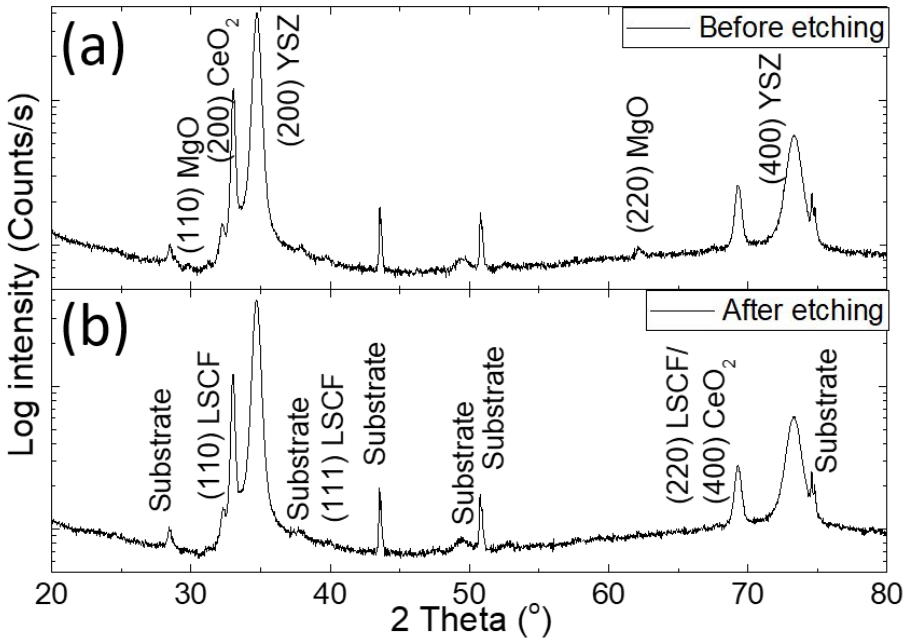

Figure S3: XRD measurements of YSZ (1500 nm) and CeO_2 (50 nm) buffered stainless steel substrates (Step 2) a) before and b) after etching

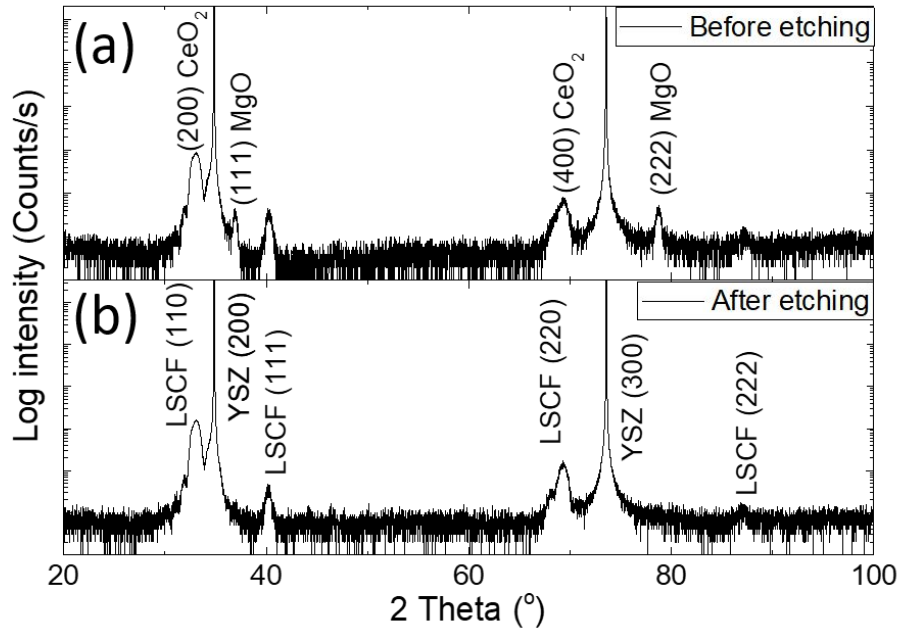

Figure S4: XRD measurements of LSCF/MgO VAN cathode on $Ce_{0.8}Gd_{0.2}O_2$-buffered single-crystal YSZ a) before and b) after etching

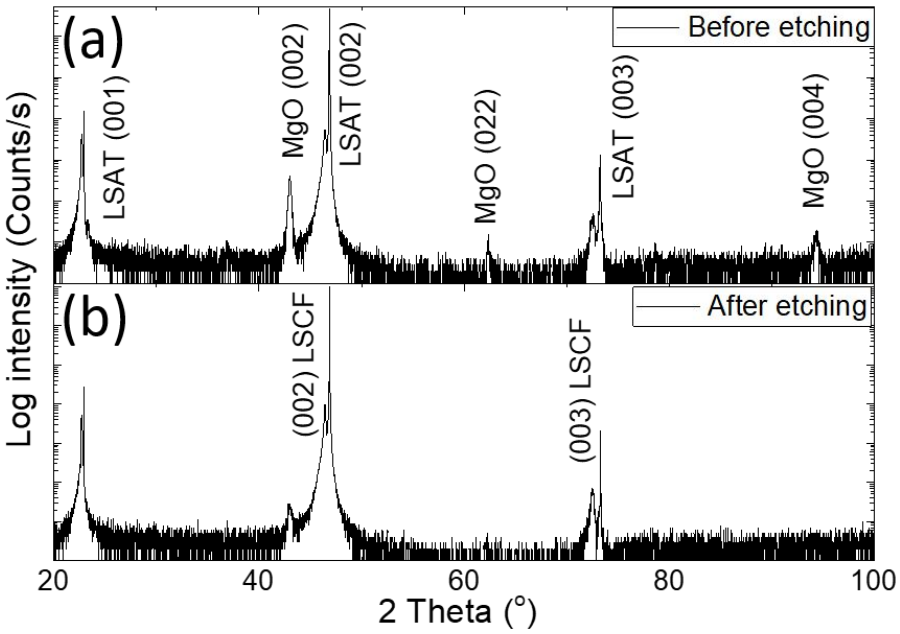

Figure S5: XRD measurements of LSCF/MgO cathode on LSAT a) before and b) after etching

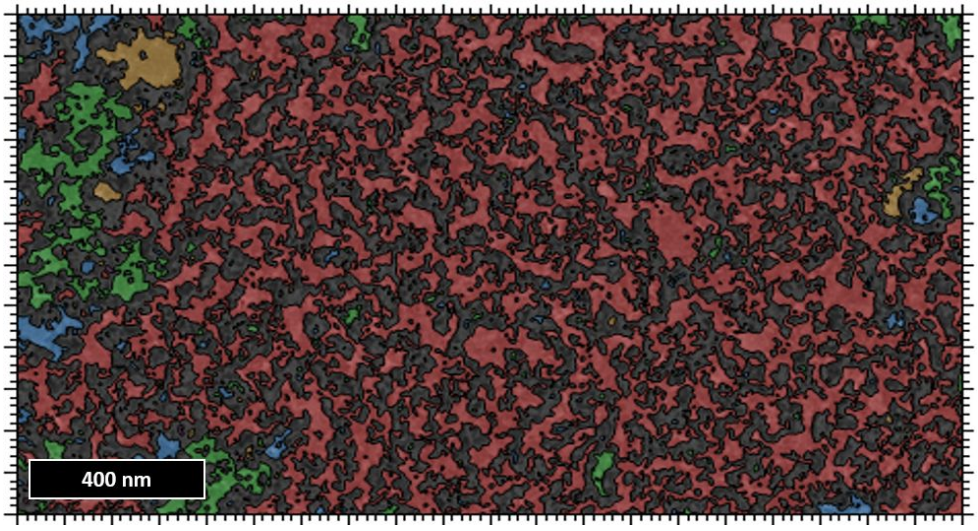

Figure S6: Porosity analysis of mesoporous LSCF on single-crystal YSZ after removal of MgO

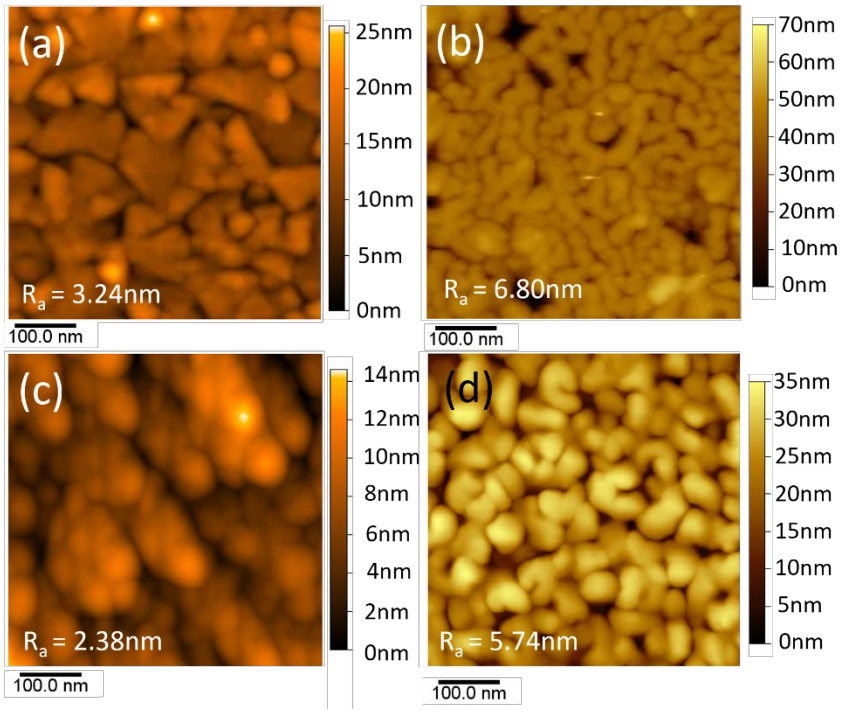

Figure S7: a) and b) AFM images of LSCF/MgO VAN films on single-crystal YSZ before and after etching of MgO, respectively. c) and d) AFM images of LSCF/MgO VAN films on ABAD-buffered stainless steel before and after etching of MgO, respectively (Step 3).

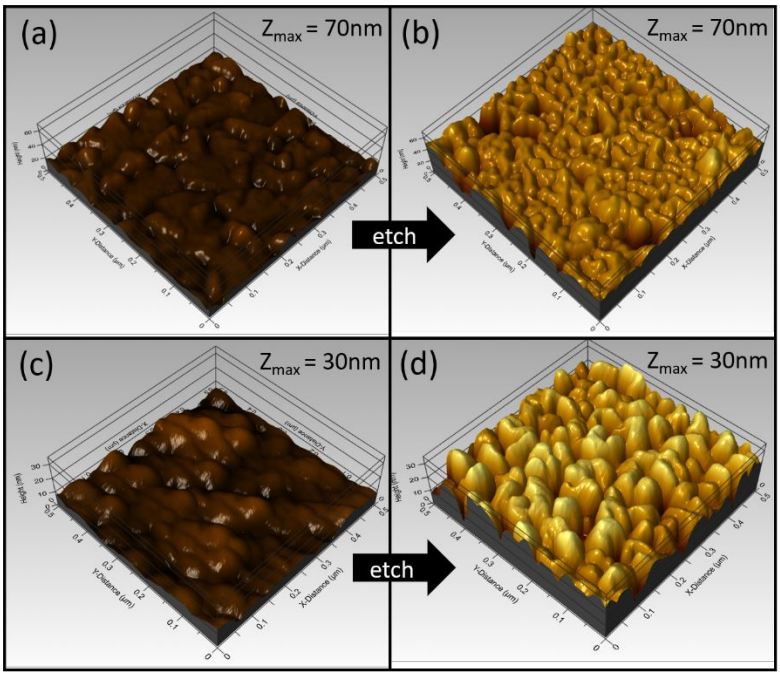

Figure S8: 3D representation of AFM images of a) and b) LSCF/MgO VAN films on single-crystal YSZ before and after etching of MgO, respectively. c) and d) AFM images of LSCF/MgO VAN films on ABAD YSZ-buffered stainless steel before and after etching of MgO, respectively.

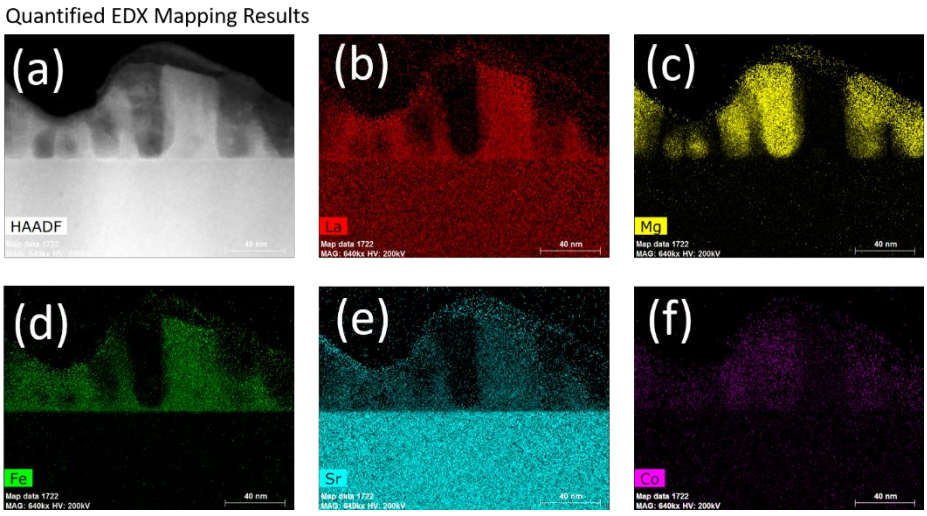

Figure S9: HAADF (a) and EDX (b-f) images of etched LSCF/MgO VAN film on LSAT, confirming phase separation and film composition (All EDX images - MAG: 640kx; HV: 200kV).

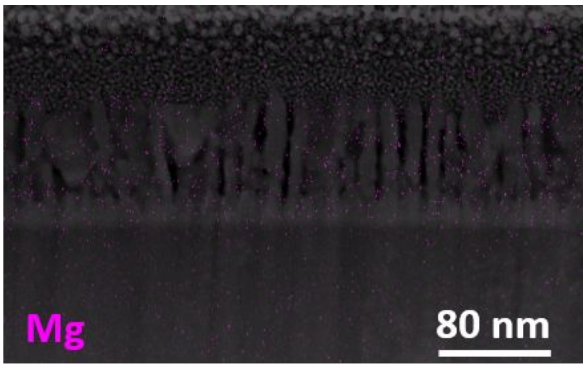

Figure S10: EDX measurements showing removal of Mg after etching for samples on ABAD-buffered metal substrates

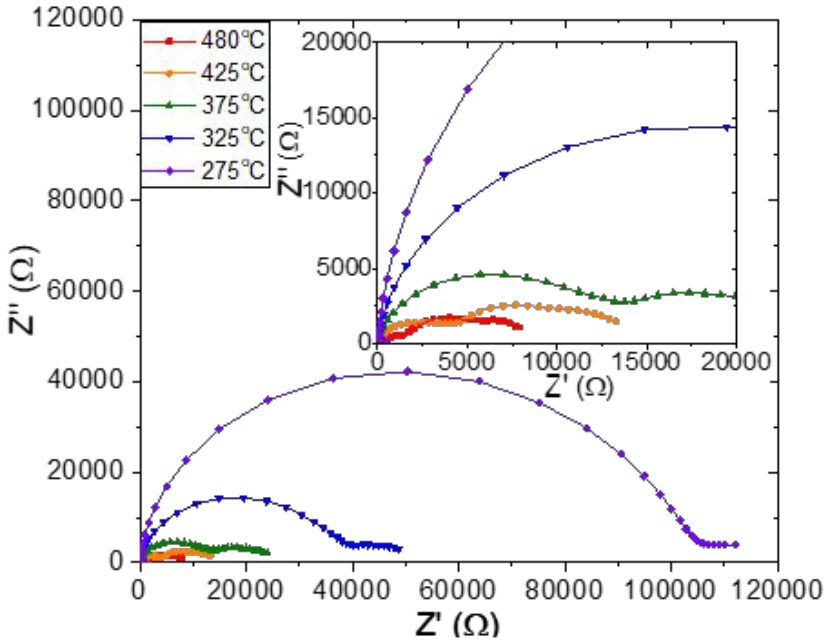

Figure S11: EIS measurements of YSZ (1500 nm) and CeO_2 (50 nm) buffered stainless steel substrates

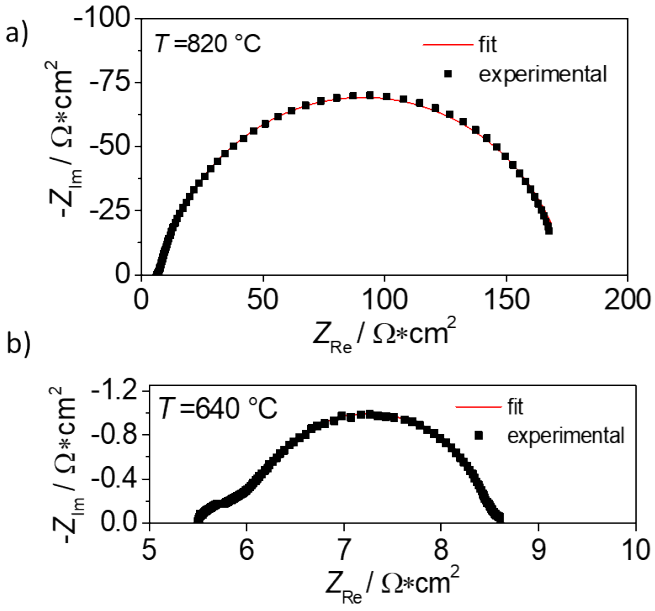

Figure S12: Representative Nyquist plots for LSCF/MgO VAN films before (a) and after (b) etching. The fitting (red line) was carried out employing an equivalent circuit with 2 ZARC elements in series. The high frequency intercept with the real axis represents the resistance of the electrolyte. The contribution of the Ag counter-electrode is negligible.

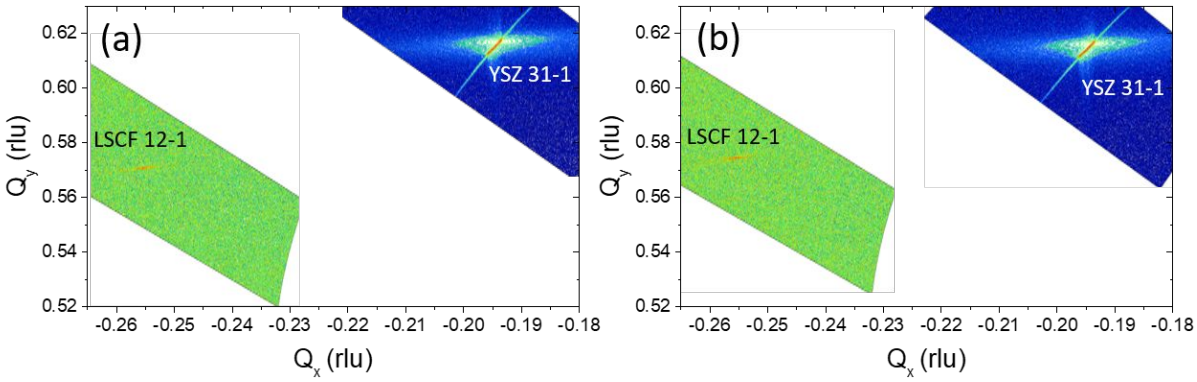

Figure S13: Reciprocal space maps for LSCF/VAN films grown on single-crystal (100) YSZ a) before and b) after etching

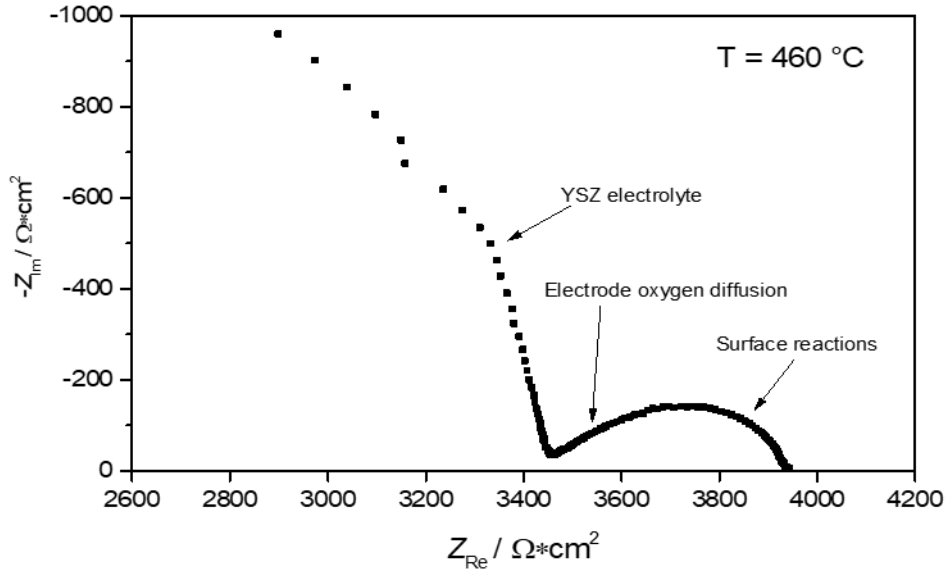

Figure S14: Distorted impedance spectrum of etched LSCF/MgO VAN film on $Ce_{0.8}Gd_{0.2}O_2$-buffered single-crystal (100) YSZ